

Elastic and inelastic scattering of 0.8 GeV protons from ^{24}Mg and ^{26}Mg

G. S. Blanpied

*University of South Carolina, Columbia, South Carolina 29208*N. M. Hintz, G. S. Kyle,* M. A. Franey, S. J. Seestrom-Morris, R. K. Owen, J. W. Palm, and D. Dehnhard
*University of Minnesota, Minneapolis, Minnesota 55455*M. L. Barlett, C. J. Harvey, G. W. Hoffmann, J. A. McGill, R. P. Liljestrand,[†] and L. Ray
University of Texas, Austin, Texas 78712

(Received 14 August 1981)

Angular distributions for the elastic and inelastic scattering of 0.8 GeV protons from ^{24}Mg and ^{26}Mg are presented. Cross sections for protons exciting states of energy up to about 10 MeV are measured using a high resolution spectrometer. Coupled channels analyses of scattering data to the 0^+ , 2^+ , 4^+ , and 6^+ states in the ground state rotational band, the 2^+ , 3^+ , 4^+ , and 6^+ states in the γ -vibrational band, the 0^+ , 2^+ , and 4^+ states in the β -vibrational band, and the 3^- and 5^- members of the $K^\pi=0^-$ and 3^- vibrational bands in ^{24}Mg are presented. Also reported are coupled channels analyses of the experimental angular distributions in ^{26}Mg for the 0^+ , 2^+ , and 4^+ states in the ground state band, the possible 2^+ , 3^+ , and 4^+ , γ -band members, and several 3^- members of $K^\pi=0^-$ and 3^- bands. The data for the 3^- states in both ^{24}Mg and ^{26}Mg differ both in shape and angular positions of the maxima and minima. Coupled channels analyses are able to account for these differences in the 3^- experimental cross sections by selecting $K^\pi=0^-$ or 3^- . This is believed to be the first observation of "K dependence" for $l=3$ excitations in inelastic scattering by s - d shell nuclei. Distorted wave Born approximation analyses of the other states in ^{26}Mg excited by l transfers from 2 to 4 are also described. Several new assignments of J^π for excited states in ^{26}Mg are proposed based upon the distinctive l transfer dependence found in the positions of the first maximum and in the general shapes of the angular distributions. Multipole moments extracted from the deformed optical potentials are related to those of the matter distributions by Satchler's theorem. These are compared to multipole moments obtained from analyses of hadronic scattering data, as well as with the moments of the charge distributions determined by electromagnetic measurements.

NUCLEAR REACTIONS $^{24,26}\text{Mg}(p,p')$, $E=0.8$ GeV, measured $\sigma(\theta)$, enriched targets; resolution ≥ 80 keV, $\theta_{\text{c.m.}}=5.49^\circ$ to 31.66° , $\Delta\theta=0.1^\circ$. Optical model potential, DWBA analysis, coupled channels analysis, symmetric and asymmetric rotational model, coupling parameters, multipole moments, assigned J^π .

I. INTRODUCTION

Coupled channels analyses of ~ 1 GeV proton inelastic scattering from light, s - d shell nuclei and heavy, rare earth nuclei have been shown to be generally successful, provided deformation and multistep processes are properly accounted for.¹⁻⁵ In particular, two recent analyses^{3,4} of preliminary 800 MeV $^{24}\text{Mg}(p,p')$ data demonstrated the applicability of the collective, rotational model to the

(0.0 MeV, 0^+), (1.37 MeV, 2^+), and (4.12 MeV, 4^+) states, and the importance of a direct hexadecupole vibrational coupling between the ground and "gamma" bands.⁴

In order to further the study of intermediate energy proton inelastic scattering from light, deformed nuclei, the preliminary data of Ref. 3 have been completed here. The final data for ^{24}Mg generally agree with the on-line data of Ref. 3, but have improved statistics, cover a more complete angular range, and include several new states. In

addition, we report new angular distributions for (p,p') from ^{26}Mg . These new data include inelastic transitions to states in $^{24,26}\text{Mg}$ which have excitation energies ranging up to about 10 MeV. The experimental data consist of angular distributions for the (ground state, 0^+), (1.37 MeV, 2^+), (4.12, 4^+), (4.24, 2^+), (5.24, 3^+), (6.01, 4^+), (6.43, 0^+), (7.35, 2^+), (7.62, 3^-), (8.12, 6^+), (8.36, 3^-), (8.44, 4^+), (9.30), (9.53, 6^+), (10.03, 5^-), (10.36), and (10.58) states in ^{24}Mg , and for the (ground state, 0^+), (1.81, 2^+), (2.94, 2^+), (3.59, 0^+), (3.94, 3^+), (4.3, $4^+ + 2^+$), (4.90, 4^+), (5.29, 2^+), (5.47, 4^+), (5.72, 4^+), (6.88, 3^-), (7.34), (7.69, 3^-), (7.83, 3^-), (8.02), (8.21), (8.50), (8.63, 4^+), (8.89), (9.25, 4^+), and (10.34, 4^+) states in ^{26}Mg .

These new data are examined in order to determine the importance of direct hexadecupole vibrational coupling between the ground and gamma bands in ^{26}Mg . Of particular interest is whether this effect, which is extremely important in $^{24}\text{Mg}(p,p')$, is also important in $^{26}\text{Mg}(p,p')$.

The multipole moments of the deformed optical potential have been extracted and related to those of the matter density by Satchler's theorem.⁶ The moments of the matter distributions in $^{24,26}\text{Mg}$ are compared to electromagnetic measurements of the charge density multipole moments.⁷⁻¹⁰ Comparisons of these quantities for ^{24}Mg and ^{26}Mg provide estimates of the change in the deformation of the neutron distributions of these isotopes. The extracted multipole moments are also compared with those obtained in other analyses of inelastic proton,¹¹⁻¹⁶ deuteron,¹⁷ ^3He ,^{18,19} and ^4He ^{19,20} scattering as well as with various theoretical predictions.^{8,9,21}

The abundant angular distributions obtained here are also exploited for their spectroscopic value. Several new J^π assignments in ^{26}Mg are proposed as a result of comparisons of the position of the first maximum and general shape of each angular distribution with theory.

The data reported here can also be utilized in future coupled-channels, microscopic analyses which examine deformed neutron distributions. It is significant to note that these are the first intermediate energy proton-deformed nucleus scattering data which are suitable for microscopic analyses aimed at the extraction of deformed, isotopic neutron distribution differences.

Experimental details are discussed in Sec. II, while the results for ^{24}Mg and ^{26}Mg are presented in Secs. III and IV, respectively. A summary and conclusions are finally given in Sec. V.

II. EXPERIMENTAL DETAILS

The data were obtained using the high resolution spectrometer (HRS) facility of the Los Alamos Clinton P. Anderson Meson Physics Facility (LAMPF). Details of the experimental system have been reported elsewhere.^{2,3,22} The targets consisted of a 19.6 mg/cm^2 ^{24}Mg foil, enriched to 99.94% and a 26.3 mg/cm^2 ^{26}Mg foil, enriched to greater than 99%. The overall experimental energy resolution was typically 80–120 keV for full HRS acceptance. A (p,p') spectrum at 29°_{lab} for ^{24}Mg is shown in Fig. 1 and a spectrum obtained at 24.5°_{lab} for ^{26}Mg is displayed in Fig. 2. These are the largest angles at which the angular distributions were measured. Data were also obtained for $p + ^{12}\text{C}$ elastic scattering. The absolute normalization was determined using the $p + ^{12}\text{C}$ data of Ref. 2.

Angular distributions for the excitation of states in ^{24}Mg are displayed in Figs. 3–8, while angular distributions for ^{26}Mg are found in Figs. 9–14. A complete tabulation of the numerical data is on deposit in PAPS.²³

The excitation energies were calibrated based on the energies of states below 6.88 MeV from Ref. 24. The energy resolution of about 100 keV allowed the unfolding of the cross sections for the (4.12, 4.24) MeV and (8.36, 8.44) MeV doublets in ^{24}Mg . The (7.55, 1^-), (7.75, 1^+), and (7.81, 5^+) peaks in the spectra were masked by the large (7.62, 3^-) peak at most angles. A 1^- state in ^{24}Mg is also unresolved from the (8.44, 4^+) state, but is probably only weakly excited, as it does not appear to wash out the fairly deep diffraction pattern that is observed here. The peak in the ^{24}Mg spectrum

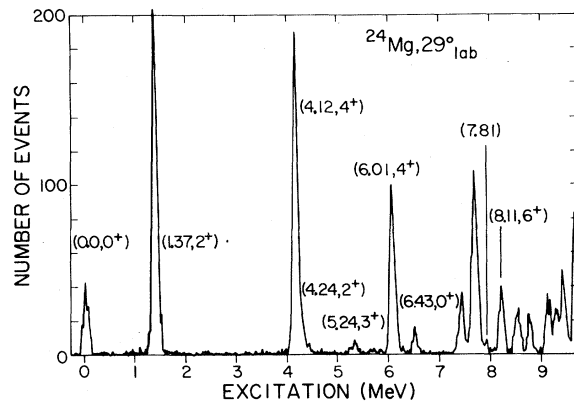


FIG. 1. The $\theta_L = 29^\circ$ spectrum for $^{24}\text{Mg}(p,p')$ at 0.8 GeV.

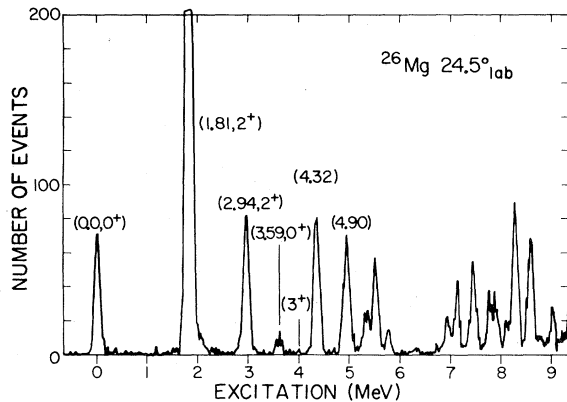


FIG. 2. The $\theta_L = 24.5^\circ$ spectrum for $^{26}\text{Mg}(p, p')$ at 0.8 GeV.

at 9.5 MeV includes contributions from the (9.46, 3^+), (9.52, 4^+ , $T=1$), and (9.52, 6^+) states. The cross section should be dominated by the 6^+ state, since at 0.8 GeV unnatural parity and isovector

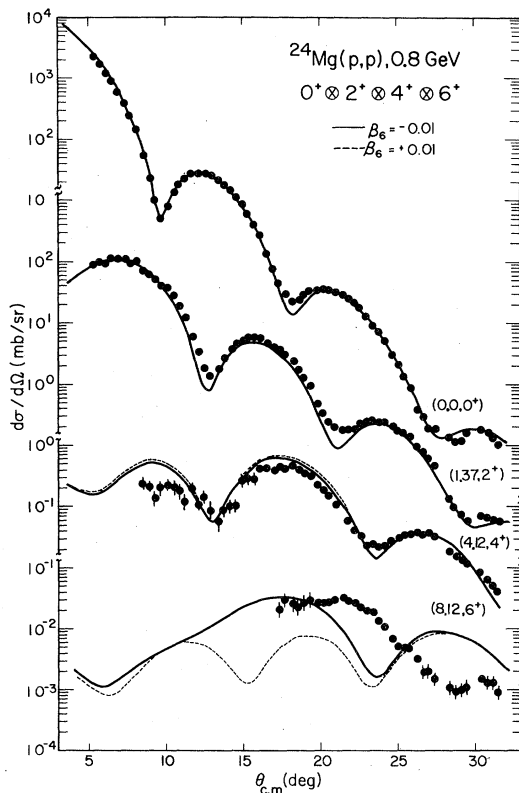


FIG. 3. Shown as solid curves are CC predictions using the axially symmetric deformed collective rotational model, and coupling the 0^+ , 2^+ , 4^+ , and 6^+ states with $\beta_2 R = 1.60$, $\beta_4 R = -0.08$ and $\beta_6 R = -0.03$ fm (solid lines), and $\beta_6 R = +0.03$ fm (dashed lines), where $R = r_w A^{1/3}$.

transitions are small compared to natural parity isoscalar transitions.

The peak at 4.3 MeV in ^{26}Mg includes contributions from the (4.32, 4^+) and the (4.33, 2^+) states and to a much less extent the (4.35, 3^+) state. The (4.90, 4^+) state appears to be resolved from the (4.83, 2^+) and (4.97, 0^+) levels. The resolution and identification of states in the region above about 7 MeV is less certain. The energies of many levels have been reported,²⁴ but few have been assigned J^π . Most of the angular distributions extracted in this region have maxima and slopes that are characteristic of a particular l transfer and are thus assumed to be dominated by a single state. Two exceptions to this are the featureless angular distributions extracted from peaks in ^{26}Mg at 8.02 and 8.89 MeV. The lack of structure in these two cross sections suggests that several states of different l transfer and comparable strength are summed in these two peaks.

III. ^{24}Mg

In this section the results of a coupled-channels (CC) analysis of most of the $^{24}\text{Mg}(p, p')$ data are given. As has been shown many times, a first order optical potential, obtained by folding the free nucleon-nucleon t matrix with the uncorrelated, one-body nuclear density, is able to provide a good description of ~ 1 GeV proton scattering from spherical nuclei.²⁵ As before,³ the assumption is made that the $p +$ deformed nucleus optical potential may be obtained, in principle, by folding a spherically symmetric proton-nucleon effective interaction $t(|\vec{r}|)$ with the deformed nuclear ground state density. Instead of obtaining this potential from a microscopic calculation, a deformed optical potential $V(\vec{r})$ was determined by fitting the elastic and inelastic scattering data for the ground state rotational band using the CC formalism, in which multistep processes are included. Then, from Satchler's theorem,⁶ the multipole moments of the matter density²⁶ were obtained from those of the optical potential. Satchler's theorem states that in units for which $\int \tilde{t} d^3r = 1$, the $M(E\lambda)$ multipole moment of $V(\vec{r})$ obtained in the folding process is equal to the same $M(E\lambda)$ of the matter density. The multipole moments of the imaginary part of the optical potential, $V(r, \theta')$ (axially symmetric in the body fixed system²⁷, are defined as²⁶

$$M(E\lambda, \text{opt. pot.}) = \frac{Ze \int r^\lambda Y_{\lambda 0}(\Omega') \text{Im}[V(r, \theta')] r^2 dr d\Omega'}{\int \text{Im}[V(r, \theta')] r^2 dr d\Omega'} \quad (1)$$

The charge of the target nucleus, Ze , is included to allow direct comparison between the optical potential quantities and the charge distribution moments. Such a comparison was made for 0.8 GeV $p + {}^{154}\text{Sm}$ and ${}^{176}\text{Yb}$, and the results agreed well with those obtained from electron scattering, Coulomb excitation, and theory.⁵

The CC calculation from which the deformed optical potential is obtained was performed using a version of the program JUPITER,²⁷ which was modified to include relativistic kinematics, intrinsic β_6 deformation, coupling potentials with $\Delta l = 2, 4, 6$, and 8, and direct $\Delta l = 4$ coupling between the ground and γ -vibrational bands.¹⁻⁴ The geometry of the optical potential is the usual Fermi form,²⁷ where the radius parameter $R(\theta')$ is

$$R(\theta') = R_0 \left[1 + \sum_{\lambda=2, \text{even}}^6 \beta_\lambda Y_{\lambda 0}(\theta') \right], \quad (2)$$

where primes denote the body fixed coordinate system.²⁷ The deformed optical potential is treated using the Legendre polynomial expansion method discussed by Tamura.²⁷

At energies near 1 GeV the spin-orbit interaction is fairly weak compared to the central term and is not important in fitting angular distributions or in extracting the underlying matter density multipole moments. This is generally true for natural parity collective states which are populated either by direct or multistep processes as explicitly shown in a recent paper.²⁸ Therefore, as in previous calculations, the spin-orbit potential is omitted here.¹⁻⁵

Other rotational bands which are built on intrinsic vibrational states are calculated by including the appropriate vibrational terms $R(\theta')$, which couple the ground band to the "vibrational" bands. The states in the γ band were assumed to correspond to so called γ vibrations in which the nucleus retains the same spheroidal equilibrium deformation, but in addition oscillates such that ellipsoidal shapes are produced ($K^\pi = 2^+$ band). States in the β band correspond to " β vibrations," in which the nucleus oscillates about a given equilibrium deformation, but always retains its axial symmetry ($K^\pi = 0^+$ band). The observed 3^- and 5^- states were assumed to belong to an octupole vibrational band with $K^\pi = 3^-$ ($J^\pi = 3^-, 4^-, 5^- \dots$) or with $K^\pi = 0^-$ ($J^\pi = 1^-, 3^-, 5^- \dots$).

A. Ground state rotational band (GSRB)

Calculations for the $(0.0, 0^+)$, $(1.37, 2^+)$, $(4.12, 4^+)$, and $(8.12, 6^+)$ states were made assuming them to be members of the GSRB, where all possible couplings through $\Delta l = 8$ are allowed between each of the four channels. The Woods-Saxon optical parameters and the ground state deformations β_2 , β_4 , and β_6 were adjusted simultaneously to optimize the fits to all four angular distributions. The β_4 and β_6 deformations are small and have little effect on the 0^+ and 2^+ angular distributions. The optimum CC fits are given by the solid lines in Fig. 3. The potential parameters, given in the low energy notation V , W , r , a , r_w , a_w , r_c , β_2 , β_4 , and β_6 , are -4.0 and 93.0 MeV, 0.940 , 0.530 , 0.940 , 0.530 , and 1.05 fm, $+0.59$ (prolate), -0.03 , and -0.01 (solid lines). The dashed lines result from a similar calculation with $\beta_6 = +0.01$. As seen in Table I, the deformation length $\beta_2 R$, where $R = r_w A^{1/3}$, agrees well with those obtained from analyses of low energy proton scattering. The surface derivative imaginary potential used in earlier analyses of ${}^{12}\text{C}$ (Refs. 1,2) and ${}^{24}\text{Mg}$ (Refs. 3,4) was not found to be necessary here. The geometry of the real optical potential has been set equal to that of the imaginary part, due to the dominance of the latter at 0.8 GeV.

The excellent fits to the 0^+ , 2^+ , and 4^+ states, as shown in Fig. 3, encourages the comparison of the extracted multipole moments [$M(E2)$ and $M(E4)$] of the imaginary part of the optical potential with those of the charge densities and with the results of other measurements and theoretical predictions. In Table II, the values of $M(E2)$ determined here are seen to agree well with those of charge densities and Hartree-Fock theory, though the agreement is not as good as that for heavy deformed nuclei (1-2%).⁵ It is difficult to assess the errors in these results. If the errors in the deformed optical potential parameters r_w , a_w , β_2 , β_4 , and β_6 are assumed to be ± 0.01 fm, ± 0.01 fm, ± 0.02 , ± 0.01 , and ± 0.02 , respectively, an rms error of 4.5% in $M(E2)$ and 17% in $M(E4)$ results. Since the absolute normalization error primarily affects only the strength of the imaginary potential W , this experimental uncertainty does not contribute significantly to the error in $M(E\lambda)$. These results suggest that analysis of 0.8 GeV $p +$ nucleus inelastic scattering data is an accurate

TABLE I. Deformation parameters used in CC calculations for (p,p') to GSRB and γ band in $^{24,26}\text{Mg}$.

Nucleus	Ground band β_2R, β_4R (fm) ^a	γ band γ, η_1R, η_2R (fm) ^b	Energy	Reference
^{24}Mg	+ 1.60, -0.081	15°, 0.42, 0.72	800	This work, 4
	+ 1.60, -0.081	20°, 0.56, 0	800	This work, 3
	+ 1.56, -0.19	22°, 0.60, 0 ^c	20	11
	+ 1.64 - 1.87, 0	23°, 0.64, 0	23-29	12
	+ 1.72, 0	23°, 0.69, 0	30	13
	+ 1.45, -0.08	21° ^d	20.5	16
	+ 1.66, -0.06	21° ^d	49.5	16
^{26}Mg	+ 1.31, -0.37	18°, 0.41, 0.41 ^e	800	This work
	+ 1.31, -0.37	21°, 0.48, 0	800	This work
	+ 1.31, -0.37	19°, 0.43, 0.21 ^{f,g}	800	This work
	+ 1.29, -0.40	25°, 0.56, 0 ^h	24	15
	+ 1.31, -0.35	29° ^d	24	16

^a $R = rA^{1/3}$, where r is that of the real part of the optical potential for low energy results, and $r = r_w$ for 800 MeV (p,p') .

^b η_1R, η_2R matrix elements are explained in text.

^cDeformed spin orbit included.

^dDirect excitation of 4_γ^+ is included in an *ad hoc* fashion. See text.

^e γ band taken to be $2^+, 3^+, 4^+ = 2.9, 3.9, 4.9$ MeV.

^f γ band taken to be $2^+, 3^+, 4^+ = 2.9, 3.9, 5.5$ MeV.

^g γ band taken to be $2^+, 3^+, 4^+ = 2.9, 4.4, 5.7$ MeV.

^hSpin orbit included. Poor fits to data result.

method for studying deformed matter distributions. However, as in Ref. 3, the CC description of the $(8.12, 6^+)$ angular distribution is very poor, even when a β_6 deformation is allowed.

B. γ band

For these calculations the $(4.24, 2^+)$, $(5.24, 3^+)$, $(6.01, 4^+)$, $(7.8, 5^+)$, and $(9.5, 6^+)$, denoted $2_\gamma^+, 3_\gamma^+$, etc., are considered to be members of the γ -vibrational band. The calculation is similar to that reported in Ref. 4, except the 6_γ^+ state is included whereas the much weaker 5_γ^+ state is omitted. Previous CC analyses of inelastic scattering data for these states in ^{24}Mg completely failed to account for the shapes and magnitudes of the 3_γ^+ and 4_γ^+ angular distributions.³ The excellent results of Ref. 4 are due to the inclusion of an additional nuclear vibrational multipole which permits a direct transition from the ground state to the 4_γ^+ member of the γ band. Equation (2) is generalized as follows:

$$R(\theta', \phi') = R_0 \left[1 + \sum_{\lambda\mu} \alpha_{\lambda\mu} Y_{\lambda\mu}(\theta', \phi') \right]. \quad (3)$$

The simplest coupling between the GSRB and the $K^\pi = 2^+$, γ band is through the $\alpha_{22}(Y_{22} + Y_{2-2})$ term, which directly excites only the 2_γ^+ member of the γ band. The additional $\alpha_{42}(Y_{42} + Y_{4-2})$ coupling permits direct transition from the ground state to the 4_γ^+ and can interfere with the α_{22} term. The matrix elements of interest, η_1 and η_2 , are defined in Ref. 4. Basically, η_1R is the matrix element of the vibrational operator α_{22} , which connects intrinsic states of the ground band to the γ band, and is approximately equal to $\beta_2\gamma R$ as in previous analyses.^{3,4} The matrix element η_2R is similarly related to the α_{42} coupling. In fitting the inelastic angular distributions, the matrix elements η_1 and η_2 are varied to produce the best overall agreement in magnitude for the $(4.24, 2^+)$ and the $(6.01, 4^+)$ states. There is no direct-step population of the $(9.53, 6^+)$ state provided here, and since spin-dependence is omitted, there is no direct spin-transfer contribution to the 3_γ^+ state. Since the α_{22}

TABLE II. Multipole moments ($eb^{\lambda/2}$).

Nucleus	$M(E2)$	$M(E4)$	$\beta_2 R^a$	$\Delta(2)^b$	Reaction	Reference
^{24}Mg	0.188	0.0073	1.60		(p,p),800	This work
	0.218±0.010	0.0041±0.0013		16%	(e,e')	7
	0.205±0.007			9%	Coulomb	9
	0.205±0.006	0.038±0.0013		9%	Coulomb	10
	0.216	0.0073	1.56	15%	(p,p),20	11 ^c
	0.216	0.0021	1.56	15%	(p,p),20	11 ^c
	0.204–0.276	0.007–0.019	1.45–1.87	9–47%	(p,p),23–29	12,16
	0.245	0.0152	1.72	30%	(p,p),30	13
	0.242–0.253	0.010–.020	1.69	29–35%	(p,p),40	14
	0.216–0.238	0.0083–0.0128	1.51–1.66	15–27%	(p,p),50	10,16
	0.199	0.0104	1.34	6%	(d,d),26	17
	0.209	0.0086	1.37	11%	(α,α),104	20
	0.184	0.0059	1.31	2%	($^3\text{He},^3\text{He}$),41	19
	0.204	0.0045	1.31	9%	(α,α),120	19
	0.203	0.0116		8%	HF-theory	21
	0.187			0%	shell model	9 ^d
	^{26}Mg	0.142	–0.0030	1.31		(p,p),800
0.178		–0.0095	1.29	25%	(p,p),24	15
0.181		–0.0073	1.31	27%	(p,p),24	16
0.172		+0.0050	1.17	21%	($^3\text{He},^3\text{He}$),33	18
0.167		+0.0032	1.09	18%	(α,α),104	20
0.172±0.008				21±6%	Coulomb	9
0.139		+0.0051	0.95	2%	(d,d),26	17
0.200				41%	HF(5 shells)	8
0.211				49%	Nilsson (7 shells)	8
0.143				<1%	triaxially deformed rotor	8
0.109				23%	HFB(3 shells)	8
0.177				25%	rotational model	9
0.175				23%	shell model	9 ^d

^a $R = rA^{1/3}$, where r is that for the real part of the optical potential for low energy, and $r = r_w$ for 800 MeV (p,p').

^b $\Delta(2) = [|M(E2) - M(E2 \text{ at } 800 \text{ MeV})| / M(E2 \text{ at } 800 \text{ MeV})] \times 100\%$.

^c β_6 varied.

^dTheoretical calculation for $B(E2)$, using effective charge of 0.35. (Ref. 9).

and α_{42} couplings can interfere, the relative sign between η_1 and η_2 is also determined by fitting the data.

The analysis of the data with $\eta_1 R = 0.56$ fm and $\eta_2 R = 0$ was shown in Refs. 3 and 4 to be exceedingly poor. The magnitude of the transition to the 2_γ^+ state was correctly obtained since it was used to fix $\eta_1 R$, but the predicted diffractive angular distribution was out-of-phase with the data by from 1° to 2° . Furthermore, the magnitudes of the 3_γ^+ and 4_γ^+ predictions were too low by factors of from 10 to 100; the predicted shapes were also wrong. As in Ref. 4, the analysis with $\eta_1 R = 0.41$

and $\eta_2 R = 0.70$ fm, given by the solid lines in Fig. 4, reproduces the data very well.

Of course, the inclusion of the adjustable α_{42} term would be expected to improve the fit to the 4_γ^+ angular distribution. As an impressive by-product, the predicted angular distribution for the 2_γ^+ state is correctly shifted into phase with the data, and the predictions of the angular distributions for the 3_γ^+ and 6_γ^+ states reproduce the magnitude and overall slope of the experimental angular distributions, although having somewhat too much structure. Direct spin-transfer contributions and additional multistep contributions from other

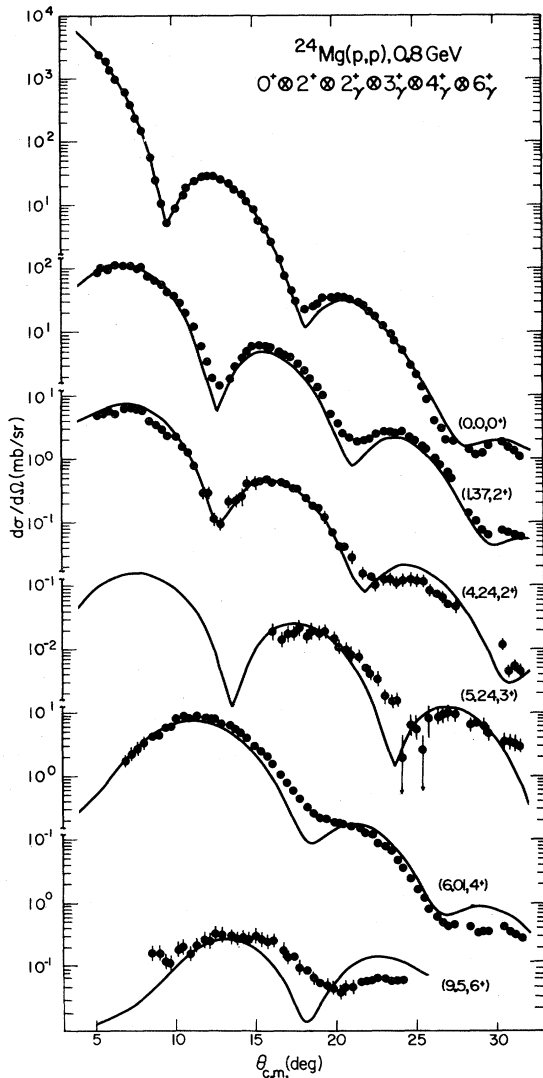


FIG. 4. The solid curves result from a CC calculation which couples the 0^+ and 2^+ states in the GSRB to the 2^+ , 3^+ , 4^+ and 6^+ , $K^\pi=2^+$ band. Additional parameters as explained in the text are $\eta_1 R = 0.41$ fm and $\eta_2 R = 0.70$ fm.

bands and higher levels would be expected to be out of phase with the two step mechanism, and thus should tend to dampen the diffractive structure. A calculation in which the 0^+ , 2^+ , and 4^+ , members of the GSRB and the 2^+ , 3^+ , and 4^+ γ -band members are all coupled demonstrates that the inclusion of the 4^+ GSRM state has no effect on the predicted angular distributions (out to 30°) for states in the γ band.

Calculations for low energy proton,¹⁶ ^3He , and ^4He (Ref. 19) inelastic scattering data for the 2^+ , 3^+ , and 4^+ states in the γ band, have been present

ed using an *ad hoc* coupling of the 4^+ to the ground state. These authors report improved fits to their data when the relative sign between η_1 and η_2 is negative. This relative sign, found here to be positive, is determined through delicate interference effects on the 2^+ angular distribution. The coupled channels calculations reported here and in Ref. 4, which include the α_{42} coupling, consistently should provide a more reliable determination of this sign. The authors of Ref. 16 and 19 do permit a different $\beta_2 Y_{20}$ deformation within the γ band than is assumed in the ground band (about 20% larger). Such a departure from the strict deformed vibrational model would mainly affect the strength of the 3^+ and 6^+ angular distributions, but owing to the fact that the overall magnitudes of these states are well reproduced in our calculations, such a change is not significant.

C. β band

The $(6.43, 0^+)$, $(7.35, 2^+)$, and $(8.44, 4^+)$ states (denoted 0^+_β , 2^+_β , 4^+_β) are assumed to be members of the β -vibrational band in ^{24}Mg in the CC calculations shown in Fig. 5. The J^π of the 8.44 MeV state is listed as either 3^+ or 4^+ in Ref. 24. Assuming $J^\pi(8.44)=4^+$ in the calculation yields the good fit to the data displayed in Fig. 5. The 8.44 MeV data are similar in shape but about 10 times stronger than the $(5.24, 3^+)$ data of Fig. 4. The CC calculation and the strength of the 8.44 MeV state suggest that it is a 4^+ state. In the present calculation the 0^+ and 2^+ members of the GSRB and the above members of the β band are coupled. Since a β vibration corresponds to an axially symmetric oscillation, the appropriate vibrational strength parameter is $|\beta - \beta_2|^3$. A value of $|\beta - \beta_2| \cdot R = 0.41$ fm ($\beta_2 R = 1.60$ fm) was found to reproduce roughly the magnitude of the angular distribution for the 0^+_β state. The quality of the fits shown in Fig. 5 is disappointing compared to those given for the γ -band states in Fig. 4. The magnitudes and overall falloff of the predictions for the states in the β band are fair, but the predictions are grossly out of phase with the data. Improvement might result if one were to include a direct step mechanism from the ground state to the 0^+_β in the CC calculations. As discussed in Ref. 3, DWBA analyses employing collective¹⁴ and shell model¹⁰ wave functions also fail to fit low energy data for this 0^+_β state.

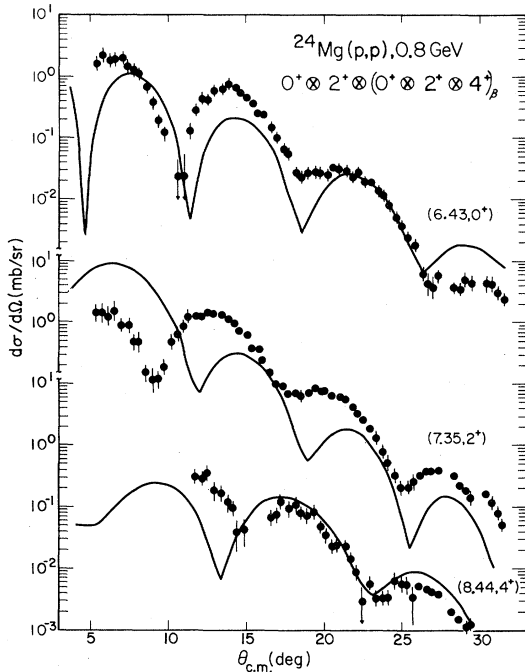


FIG. 5. The angular distributions for excitation of the β band in ^{24}Mg are compared to a CC prediction which couples the 0^+ and 2^+ states in the GSRB and the 0^+ , 2^+ , and 4^+ , $K^\pi=0^+$ states. The β -vibrational parameter is $|\beta-\beta_2|\cdot R=0.41$ fm.

D. $K^\pi=0^-, 3^-$ bands

Data for the excitation of the $(7.62, 3^-)$, $(8.36, 3^-)$, and $(10.02, 5^-)$ states in ^{24}Mg are presented in Fig. 6. Based upon the known energies and J^π values of states in ^{24}Mg , K^π -band assignments are made in Ref. 24, which lists the $(7.55, 1^-)$, $(8.36, 3^-)$, $(10.03, 5^-)$ and $(12.42, 7^-)$ states as belonging to a $K^\pi=0^-$ band, while the $(7.62, 3^-)$, $(9.30, 4^-)$, and $(11.59, 5^-)$ states are listed as members of a $K^\pi=3^-$ band.²⁴ The $(7.55, 1^-)$ state is not resolved in this experiment and the $(12.42, 7^-)$ state, although observed in the spectra, could not be extracted due to background uncertainties and proximity to the edge of the focal plane.

The striking differences in the angular distributions of the two 3^- states shown in Fig. 6 are readily apparent. The minimum of the 8.36 MeV data is located at a much smaller angle than that for the 7.62 MeV state, and the first maximum for the 7.62 MeV data is much broader than that for the 8.36 MeV state. CC calculations in which the 0^+ and 2^+ states of the GSRB are coupled to an octupole vibrational band with either $K^\pi=0^-$ or 3^- are shown in the figure. In each calculation

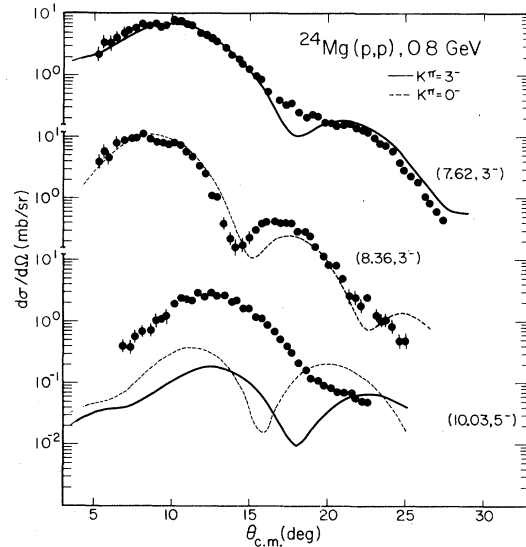


FIG. 6. The results of CC calculations which couple the 0^+ and 2^+ states in the GSRB to a $K^\pi=0^-$ band ($1^-, 3^-, 5^- \dots$), and to a $K^\pi=3^-$ band ($3^-, 4^-, 5^- \dots$). The $(7.62, 3^-)$ state is considered to belong to a 3^- band ($\alpha_{33}R=0.89$ fm) and the $(8.36, 3^-)$ state to a 0^- band ($\alpha_{30}R=0.60$ fm). The curves for the $(10.03, 5^-)$ state result from consideration of the state as a member of the 0^- band (solid curve) and the 3^- band (dashed curve). There is no direct step provided to the 5^- state from the ground state in either calculation.

the $(10.03, 5^-)$ state is also coupled, but with no direct step from the ground state allowed. The dashed curves in Fig. 6 for the $(8.36, 3^-)$ and $(10.03, 5^-)$ state are the result of considering them to be members of a $K^\pi=0^-$ octupole vibrational band, while the solid curves for the $(7.62, 3^-)$ and the 5^- state are the result of considering them to be members of a $K^\pi=3^-$ band. Although the fits are not perfect, they do account for the qualitative differences in the 3^- cross sections. Both calculations grossly underestimate the 5^- cross section, suggesting that a direct ground state to 5^- coupling might be needed to explain the data.

This is believed to be the first observation of K dependence for $l=3$ excitations in inelastic scattering in s - d shell nuclei. A similar effect is also seen in ^{26}Mg and will be discussed in the next section. The vibrational multipoles which excite these bands are from Eq. (3), $\alpha_{30}Y_{30}$ for the $K^\pi=0^-$ band and the $\alpha_{33}(Y_{33}+Y_{3-3})$ for the 3^- band. The coupling matrix elements used in the CC calculations in Fig. 6 are $\langle\alpha_{30}\rangle R=0.60$ fm and $\langle\alpha_{33}\rangle R=0.89$ fm.

In octupole vibrational bands, two other possibil-

ities of K^π exist, namely $K^\pi=1^-$ or 2^- . The differences in the $J^\pi=3^-$ angular distributions for different K^π were explored in the CC calculations represented by the labeled lines in Fig. 7. Coupling the 0^+ and 2^+ GSRB states and a 3^- state with $K^\pi=0^-, 1^-, 2^-,$ and 3^- with $\langle\alpha_{3K}\rangle R=0.47, 0.49, 0.57,$ and 0.80 fm, respectively (to give the same cross section magnitude at 10° c.m.), has been assumed. As seen in the figure, the angular distributions for $J^\pi=3^-$ and $K^\pi=0^-$ or 1^- are very similar, while the minima for the $K^\pi=2^-$ and 3^- are shifted towards larger scattering angle.

E. Other states

Experimental angular distributions for excitation of states at 9.30, 10.36, and 10.58 MeV are given in Fig. 8. Reference 24 lists three states at approximately 9.3 MeV excitation: $(9.28, 2^+)$, $[9.30, (3,4)]$, and $[9.31, (3-5)^-]$. The observed angular distribution is similar in shape and magnitude to that of the $(6.43, 0^+)$ state in Fig. 5, and this is not characteristic of the above angular momenta. The well defined minimum in the angular distribution suggests that one transition predominates here. Inelastic electron scattering for $q \leq 1.1$ fm $^{-1}$ indicated either $l=2$ or 0 for this level and provided evidence for four states at about 9.30 MeV.²⁹

Reference 24 lists a 4^+ state at 10.33 MeV and a 2^+ state at 10.35 MeV. DWBA calculations using a spherically symmetric optical potential with parameters $V, W, W_D, r, a, r_w, a_w, r_D, a_D,$ and r_C equal to $-5.3, 88.0,$ and 8.5 MeV and $0.928, 0.621, 0.928, 0.621, 0.42, 0.47,$ and 1.05 fm, respec-

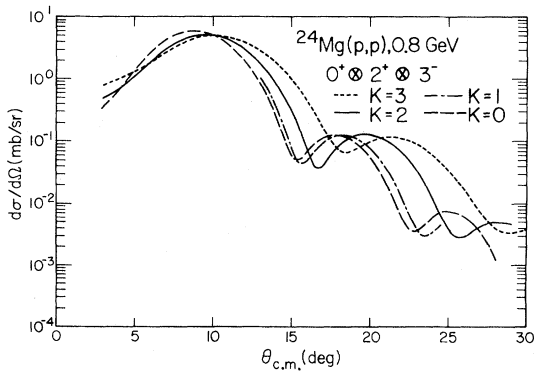


FIG. 7. The results of CC calculations coupling the 0^+ and 2^+ states in the GSRB and a 3^- state assumed to belong to a $K^\pi=0^-, 1^-, 2^-, 3^-$ band. The coupling parameters are fixed at 0.47, 0.49, 0.57, and 0.80 fm to give the same cross section at 10° (5.0 mb/sr).

tively, were made assuming $J^\pi=2^+$ and 4^+ . No combination of the 2^+ and 4^+ DWBA calculations is able to fit the data at 10.36 MeV excitation. The angular distribution has a shallow overall slope suggesting the possible importance of two-step processes.

The angular distribution for the peak at 10.58 MeV is probably the $[10.57, (2-4)^+]$ state of Ref. 24. The DWBA calculation in the figure which explains the data is $l=4$, with $|\beta_4 R|=0.22$ fm.

IV. ^{26}Mg

The excited state structure of ^{26}Mg is quite different from that discussed above for ^{24}Mg . For instance, the clear band structure in ^{24}Mg is not readily apparent in ^{26}Mg . Also, no excitations with $J > 4$ are observed. The collective $K^\pi=2^+, J^\pi=4^+$ strength is apparently fractionated among various 4^+ levels.

The complicated level structure in ^{28}Mg makes unique assignment of the various excited levels to particular rotational bands very difficult. Comparing the ordering and spacing of the excited states of ^{26}Mg with that in ^{24}Mg one could assign the $(0.0, 0^+)$, $(1.81, 2^+)$, and $(4.3, 4^+)$ states to the GSRB and the $(2.94, 2^+)$, $(3.94, 3^+)$, and $(4.9, 4^+)$ states to the γ band. However, gamma-ray angular

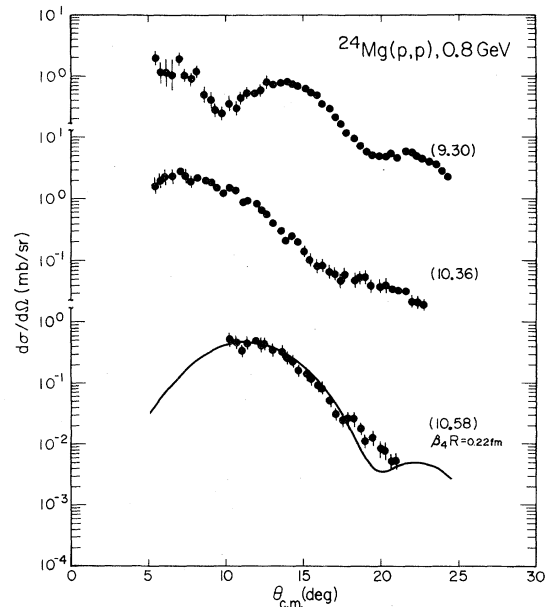


FIG. 8. Angular distribution for excitation of states at 9.30, 10.36, and 10.58 MeV in ^{24}Mg .

correlation measurements using the reactions $^{26}\text{Mg}(\alpha, \alpha'\gamma)$ and $^{26}\text{Mg}(p, p'\gamma)$ yield different, conflicting band assignments.³⁰⁻³²

Durrell *et al.*³⁰ reported that the GSRB consists of the $(0.0, 0^+)$, $(1.81, 2^+)$, and $(4.32, 4^+)$ states; the $K^\pi=2^+$ band is comprised of the $(2.94, 2^+)$, $(3.94, 3^+)$, and $(5.47, 4^+)$ states and a $K^\pi=3^+$ band that includes the $(4.35, 3^+)$ and $(5.72, 4^+)$ states. Nagel *et al.*³¹ obtained the same GSRB, but assigned the $(2.94, 2^+)$, $(4.35, 3^+)$, and $(5.72, 4^+)$ states to the $K^\pi=2^+$ band and the $(3.94, 3^+)$ and $(5.47, 4^+)$ states to the $K^\pi=3^+$ band. The complicated excited state structure for ^{26}Mg suggests that the simple deformed-vibrational collective model may be inappropriate. The possibility of K mixing in these excited states is discussed by Nagel *et al.*³² and by Craig.³³

Calculations are now presented in which each of the above choices of band assignments is assumed. The possibility of K mixing and other departures from the strict deformed-vibrational collective model is beyond the scope of the present study.

A. Ground state rotational band

Calculations for elastic scattering and inelastic transitions to the $(0.0, 0^+)$, $(1.81, 2^+)$, and $(4.3, 4^+)$ states were carried out assuming them to be members of the GSRB, with full coupling between all three channels (0^+ , 2^+ , 4^+) included. The Woods-Saxon optical potential and the ground state β_2 and β_4 deformations were adjusted to optimize simultaneously the fits to the 0^+ , 2^+ , and 4^+ angular distributions. The resulting CC predictions are given by the solid lines in Fig. 9. The potential parameters V , W , r , a , r_w , a_w , r_c , are -8.0 and 88.0 MeV and $0.950, 0.453, 0.962, 0.520$, and 1.05 fm. The deformation parameters β_2 and β_4 are 0.46 and -0.13 , while the deformation lengths are $\beta_2 R = 1.31$ fm and $\beta_4 R = -0.37$ fm, respectively. As seen in Table I, both deformation lengths agree with that obtained in analyses of low energy proton data. As seen in the figure, the fits to the 0^+ and 2^+ states are good. The differences between theory and experiment for the 4.3 MeV state are due principally to the $(4.3, 2^+)$ mixture. The 2^+ angular distribution accounts for most of the observed strength inside 10° and has a minimum near the maximum in the 4^+ cross section.

The extracted multipole moments of the imaginary part of the optical potential are given in

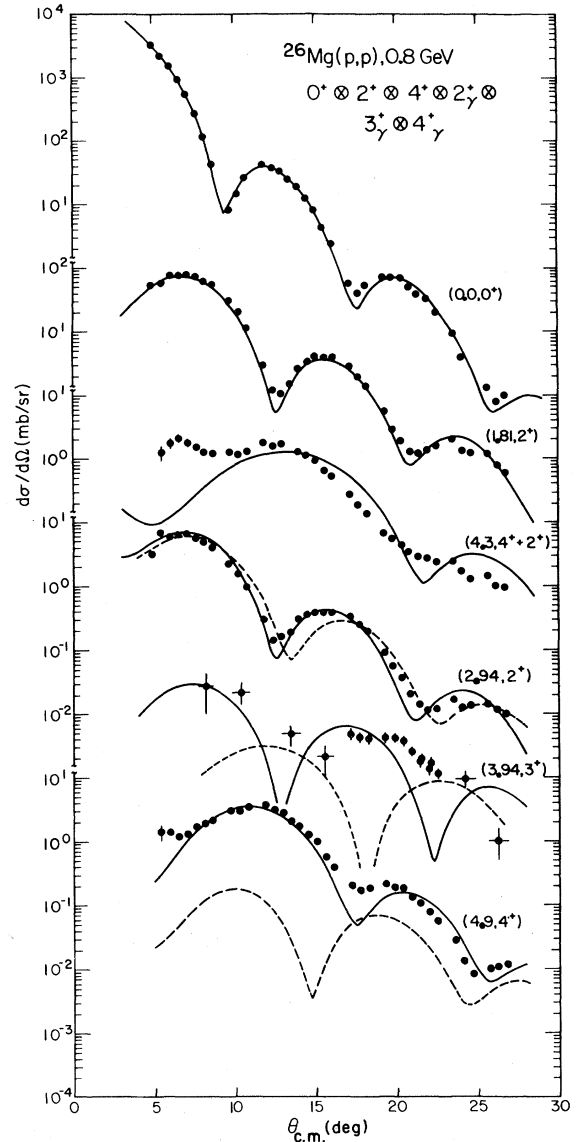


FIG. 9. Experimental angular distributions and CC predictions for protons exciting the ground state band (0^+ , 2^+ , 4^+) and $K^\pi=2^+$, γ band (2^+ , 3^+ , 4^+) in which all states are coupled. The coupling parameters are $\beta_2 R$, $\beta_4 R$, $\eta_1 R$, $\eta_2 R = +1.31, -0.37, 0.41, 0.41$ fm (solid curves), and $= +1.31, -0.37, 0.48, 0.0$ fm (dashed curves). The curve for the 4.3 MeV transition accounts for the 4^+ state only.

Table II. The results are smaller than those of low energy proton and alpha scattering. It is interesting to compare the charge, matter, and neutron density $M(E2)$ moments in ^{24}Mg and ^{26}Mg . If it is assumed that the optical potential can be obtained by folding the proton-nucleon effective interaction \tilde{t}_{pj} (j =target proton or neutron), with the target nucleon density $\rho_j(\vec{r})$ (summed over target

protons and neutrons), then the multipole moment of the deformed neutron distribution is given by

$$M(E\lambda, \text{neutron}) = \left[\left(\frac{A + N\delta}{Ze} \right) M(E\lambda, \text{opt. pot.}) - \left(\frac{1}{e} \right) M(E\lambda, \text{charge}) \right] (1 + \delta)^{-1}, \quad (4)$$

where $M(E\lambda, \text{opt. pot.})$ is given by Eq. (1), $M(E\lambda, \text{charge})$ is the multipole moment of the charge density, A , N , and Z are the target nucleus mass, neutron, and proton numbers, respectively, and δ is

given by

$$\delta = \frac{I_m \langle \tilde{t}_{pn} \rangle}{I_m \langle \tilde{t}_{pp} \rangle} - 1 = \frac{\sigma_{pn}}{\sigma_{pp}} - 1. \quad (5)$$

$I_m \langle \tilde{t}_{pj} \rangle$ denotes the volume of the imaginary part of the proton-nucleon effective interaction which in the impulse approximation²⁵ is proportional to the free proton-nucleon total cross sections σ_{pj} . At 800 MeV, δ is equal to -0.2 .²⁵

The value of $M(E2, \text{charge})$ for ^{24}Mg from Ref. 9 is 0.205 ± 0.007 e b, while $M(E2, \text{charge})$ for ^{26}Mg is 0.172 ± 0.008 e b according to the same reference. Assuming these values and assigning a

TABLE III. Excited states of ^{26}Mg .

Endt and Van der Leun (Ref. 24) E (MeV), J^π	(e, e') (Ref. 8) E, J^π	Present work (DWBA) E^a, l transfer, $\beta_1 R_n$ (fm)
1.81, 2 ⁺	1.81, 2 ⁺	2, 1.47
2.94, 2 ⁺	2.95 ± 0.01, 2 ⁺	2, 0.42
3.59, 0 ⁺	3.58 ± 0.01, 0 ⁺	0, —
3.94, 3 ⁺		Two step
4.32, 4 ⁺		4, 0.45
4.33, 2 ⁺	4.34 ± 0.03, 2 ⁺	2, 0.23
4.35, 3 ⁺		Two step
4.83, 2 ⁺		
4.90, 4 ⁺	4.88 ± 0.02, 4 ⁺	4, 0.61
4.97, 0 ⁺	4.98 ± 0.02, 0 ⁺	
5.29, 2 ⁺	5.29 ± 0.2, 2 ⁺	2, 0.25 ^b
5.47, 4 ⁺	5.45 ± 0.05, 4 ⁺	4, 0.34
5.72, 4 ⁺	5.72 ± 0.02, 4 ⁺	4, 0.36
6.88, 3 ⁻	6.88 ± 0.01, 3 ⁻	3, 0.56
7.35, 7.37	7.36 ± 0.02, 2 ⁺	7.34 ± 0.02, 2, 0.44
7.67, 7.69, 7.72	7.69 ± 0.02, 3 ⁻	7.69 ± 0.02, 3, 0.30
7.82, 7.83, 7.85	7.83 ± 0.02, 3 ⁻	7.83 ± 0.02, 3, 0.45
8.03, 8.05		8.02 ± 0.02 ^c
8.18, 8.20, (2-6) ^{Nat}	8.19 ± 0.02, 3 ⁻	8.21 ± 0.03, 0.53
8.46, 8.47, (2-6) ^{Nat}	8.53 ± 0.02, 2 ⁺	8.50 ± 0.03, 2, 0.19 ^b
8.50, 8.53		
8.70, (2-4) ^{Nat}		8.63 ± 0.03, 4, 0.25
8.86, 8.90, 8.93	8.89 ± 0.01, 2 ⁺	8.89 ± 0.03, ^c
9.24, 9.26, 9.28 ^d	9.29 ± 0.02, 2 ⁺	9.25 ± 0.03, 4, 0.36
10.32, 10.33, 10.34, ^d	10.33 ± 0.02, 3 ⁻	10.34 ± 0.04, 4, 0.49
10.35, 10.37		
10.64, 10.68, 10.69 ^d	10.68 ± 0.03, 4 ⁺	
10.70, 10.72		

^a0.0 to 6.88 MeV states from Endt and Van der Leun (Ref. 24) have been used for calibration in the present work.

^bPoor fit, two step, and deformation seem to be important.

^cMore than one level seems to be excited.

^dFrom C. E. Moss, Nucl. Phys. **A269**, 429 (1976).

$\pm 5\%$ uncertainty to the optical potential multipole moments of Table II, due to optical model ambiguities, the values of $M(E2, \text{neutron})$ are 0.167 ± 0.022 and 0.128 ± 0.020 b in ^{24}Mg and ^{26}Mg , respectively. The ratios of the $M(E2)$ moments for ^{26}Mg to those for ^{24}Mg are 0.84 ± 0.05 for the protons and 0.77 ± 0.16 for the neutrons. Thus, the inferred quadrupole moments of the proton and neutron densities are both reduced in ^{26}Mg relative to ^{24}Mg . The neutron deformation appears to be slightly less than that for the protons in ^{26}Mg ; however, the uncertainties preclude a definitive conclusion. The ratio of the neutron to proton $M(E2)$ for ^{26}Mg is 0.74 ± 0.12 , in agreement with that found from γ decay rates in mirror nuclei.³⁴ We note, however, that this same ratio for the $N=Z$ nucleus ^{24}Mg is 0.81 ± 0.11 .

B. γ -band

Initially, the $(2.94, 2^+)$, $(3.94, 3^+)$, and $(4.9, 4^+)$ states, denoted as 2_γ^+ , 3_γ^+ , and 4_γ^+ , are assumed to be members of the γ -band. The 0^+ , 2^+ , and 4^+ members of the GSRB and the 2_γ^+ , 3_γ^+ , and 4_γ^+ states are coupled using the same deformed optical potential used for the preceding GSRB calculation, but with $\eta_1 R = 0.41$ fm and $\eta_2 R = 0.41$ fm. The results are given by the solid lines in Fig. 9. The dashed lines result from assuming $\eta_1 R = 0.48$ fm and $\eta_2 R = 0$. As was the case for ^{24}Mg , including the $\alpha_{42}(Y_{42} + Y_{4-2})$ vibrational multipole provides a good fit to the 4_γ^+ , shifts the predicted cross section for the 2_γ^+ into phase with the data, and qualitatively describes the 3_γ^+ data. Additional spin-transfer transitions to the 3_γ^+ might improve the theoretical description of these data.

The calculation was then repeated assuming the $K^\pi = 2^+$ states to be the $(2.94, 2^+)$, $(3.94, 3^+)$, and $(5.47, 4^+)$ as given by the γ -ray results of Ref. 30. The results of the calculation with $\eta_1 R = 0.43$ fm and $\eta_2 R = 0.21$ fm are presented by the solid lines in Fig. 10. These fits to the γ -band data are clearly inferior to those displayed in Fig. 9. The calculated angular distributions for the 2_γ^+ and 4_γ^+ are out of phase with the data, being as much as 3° out of phase for the $(5.47, 4^+)$ state.

A similar result is shown in Fig. 11, in which the $(2.94, 2^+)$, $(4.43, 3^+)$, and $(5.72, 4^+)$ states are considered to be $K^\pi = 2^+$ band members. The coupling parameters are again $\eta_1 R = 0.43$ fm and $\eta_2 R = 0.21$ fm. The fit to the data for the 2_γ^+ state is unchanged from that in the preceding calculation and the fit to the 4_γ^+ state is also inferior

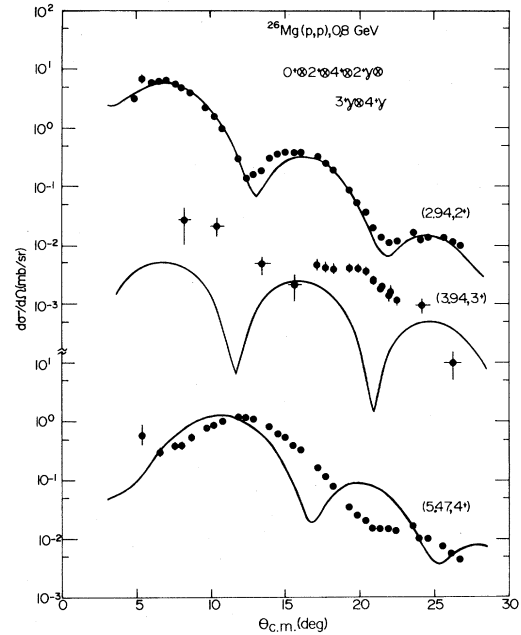


FIG. 10. Same as Fig. 9 except the $(5.47, 4^+)$ state is assumed to belong to the γ band and $\eta_1 R = 0.43$ fm and $\eta_2 R = 0.21$ fm.

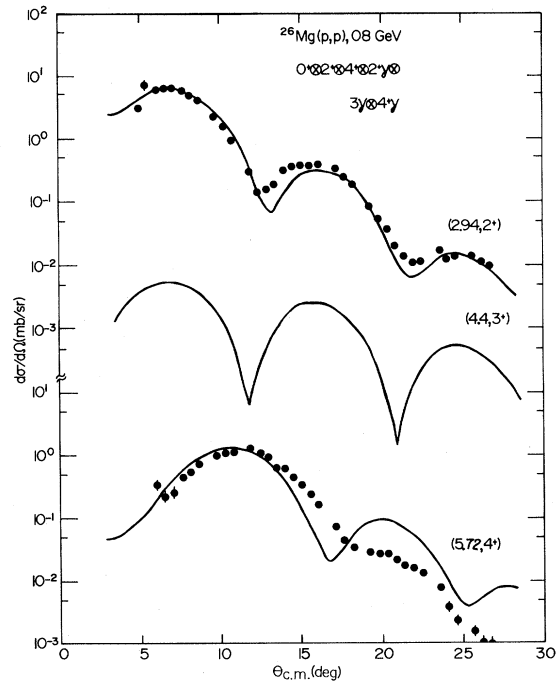


FIG. 11. Same as Fig. 9 except the $(5.72, 4^+)$ and $(4.43, 3^+)$ states are assumed to belong to the γ band and $\eta_1 R = 0.43$ fm and $\eta_2 R = 0.21$ fm.

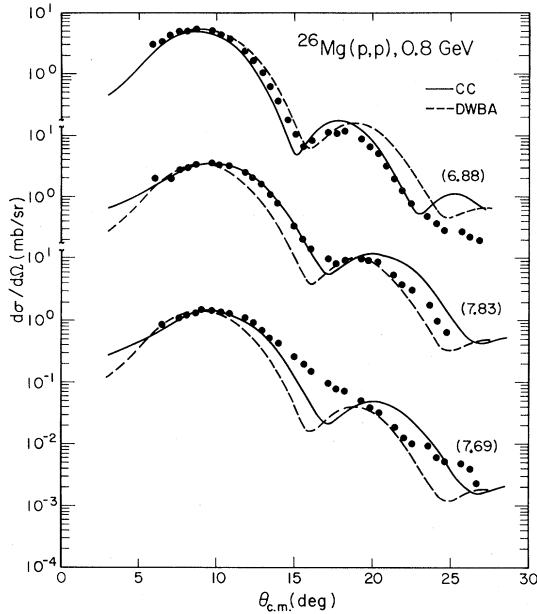


FIG. 12. Experimental angular distributions, CC, and DWBA predictions for $l=3$ excitations in ^{26}Mg . The CC calculations couple the 0^+ and 2^+ states in the GSRB and the 3^- state where $K^\pi=0^-, 3^-,$ and 3^- , and the coupling parameters are 0.43, 0.57, and 0.37 fm for the 6.88, 7.83, and 7.69 MeV states, respectively.

compared to that initially obtained for the (4.9, 4^+) state.

The importance of K -mixing in ^{26}Mg remains to be determined. It is perhaps possible that microscopic calculations using shell model wave functions can account for the variation in magnitude and shape between these three 4^+ states.

C. $K^\pi=0^-, 3^-$ bands

Angular distributions for the excitation of the 6.88, 7.69, and 7.83 MeV states are presented in Fig. 12. All three states were determined to be $J^\pi=3^-$ in (e, e') analyses,⁸ and the angular distributions here are characteristic of $l=3$. The dashed lines are the results of DWBA analyses with the spherically symmetric potential whose parameters $V, W, r, a, r_w, a_w, r_C$, are -7.6 and 66.7 MeV, and $1.028, 0.569, 0.989, 0.569,$ and 1.05 fm, respectively. The deformation lengths $|\beta_3 R|$ are 0.56, 0.45, and 0.30 fm for the 6.88, 7.83, and 7.69 MeV states, respectively. Except for the overall normalization, the DWBA calculations for each of the 3^- states are, of course identical, and do not explain either of these three sets of data.

The results of CC calculations in which the 0^+ and 2^+ states in the GSRB are coupled to a 3^- state in either a $K^\pi=0^-$ or 3^- band are shown as solid lines in the figure. Assuming $K^\pi=0^-$, the CC calculation is able to reproduce the angular distribution data for the 6.88 MeV state while assuming $K^\pi=3^-$ yields good results for the 7.83 MeV state, and fair results for the 7.69 MeV state. The coupling matrix elements for these cases are 0.43, 0.57, and 0.37 fm for the 6.88, 7.83, and 7.69 MeV states, respectively. As was the case for ^{24}Mg , the qualitative differences between the 6.88 and 7.83 MeV, $l=3$ excitations are explained by the CC calculations assuming either an α_{30} coupling term ($K^\pi=0^-$) or an α_{33} term ($K^\pi=3^-$).

D. Other states

DWBA calculations using the spherically symmetric optical potential listed in the preceding paragraph are shown for various angular distributions in Figs. 13 and 14. The results are summarized in Table III. Measured angular distributions and computed $l=4$ transitions are shown in Fig. 13, for the 4.3, 4.9, 5.47, 5.72, 8.63, and 10.34 MeV states. A similar $l=4$ calculation is given by the dot-dashed curve for the 9.25 MeV state in Fig. 14. An $l=2$ transition with $|\beta_2 R|=0.23$ fm is added incoherently to the $l=4$ DWBA transition and compared to the summed 2^+ and 4^+ states at 4.3 MeV. The DWBA calculations are able to reproduce the data in the region of the first maximum for all seven states. The remaining differences at larger angles can probably be attributed to deformation and multistep effects, as well as to deviations from the collective model. The deformation lengths $|\beta_4 R|$ are 0.45, 0.61, 0.34, 0.36, 0.25, 0.36, and 0.49 fm for the 4.3, 4.9, 5.47, 5.72, 8.63, 9.25, and 10.34 MeV states, respectively. Based upon these results the 8.63, 9.25, and 10.34 MeV states are assigned $J^\pi=4^+$.

In addition to the 9.25 MeV state, angular distributions for the (3.59, 0^+), (5.29, 2^+), (7.34), (8.02), (8.21), (8.50), and (8.99) states are given in Fig. 14. DWBA calculations are given by the dashed lines in the figure. The (3.59, 0^+) state is presumably the bandhead of a β vibrational band. The earlier CC results for the β -band in ^{24}Mg discouraged similar CC calculations for this band in ^{26}Mg . The calculations for the 5.29, 7.34, and 8.50 MeV states assume $l=2$ with $|\beta_2 R|=0.25, 0.44,$ and 0.19 fm. The fit to the data for the 7.34 MeV state is good, while that for the other two states is

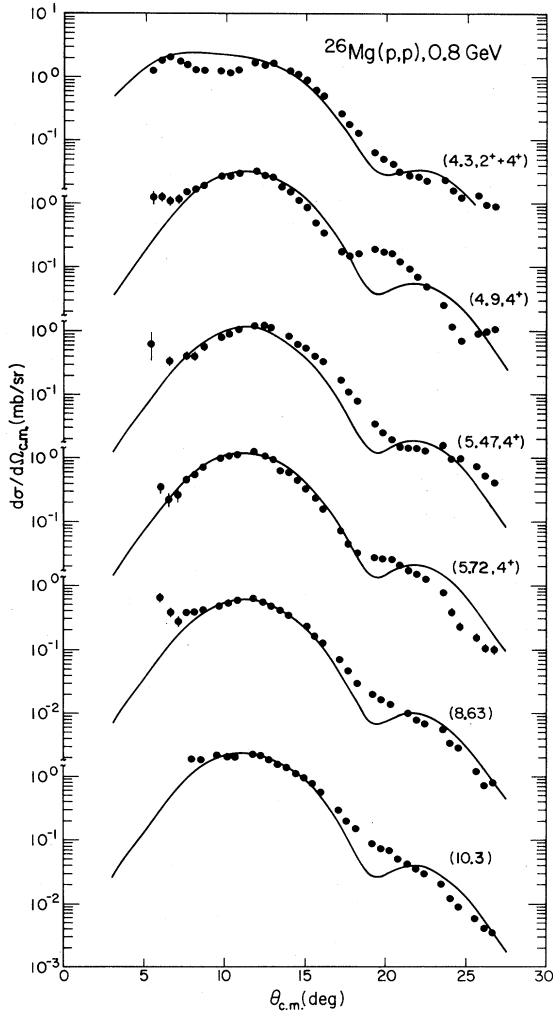


FIG. 13. Experimental angular distributions and DWBA predictions for $l=4$ excitations in ^{26}Mg . The deformation parameters for the spherical optical potential are $|\beta_4 R| = 0.45, 0.61, 0.34, 0.36, 0.25, \text{ and } 0.49$ fm for the 4.3, 4.9, 5.47, 5.72, 8.63, and 10.34 MeV states, respectively. There is an additional $l=2$, transition with $|\beta_2 R| = 0.23$ fm added to the 4.3 MeV $l=4$ DWBA angular distribution.

poor. The difference in phase and overall slope for the 5.29 and 8.50 MeV data suggests the importance of multistep contributions to these angular distributions. The DWBA calculations for the transitions to the 8.21 and 9.25 MeV states (dashed lines) assume $l=3$. The $l=4$ transition (dot-dashed curve) for the 9.25 MeV state is clearly preferred over that for $l=3$. The description of the 8.21 MeV state is fair with $|\beta_3 R| = 0.53$ fm. The lack of structure seen in the angular distribution data for the 8.02 and 8.89 MeV peaks may indicate that

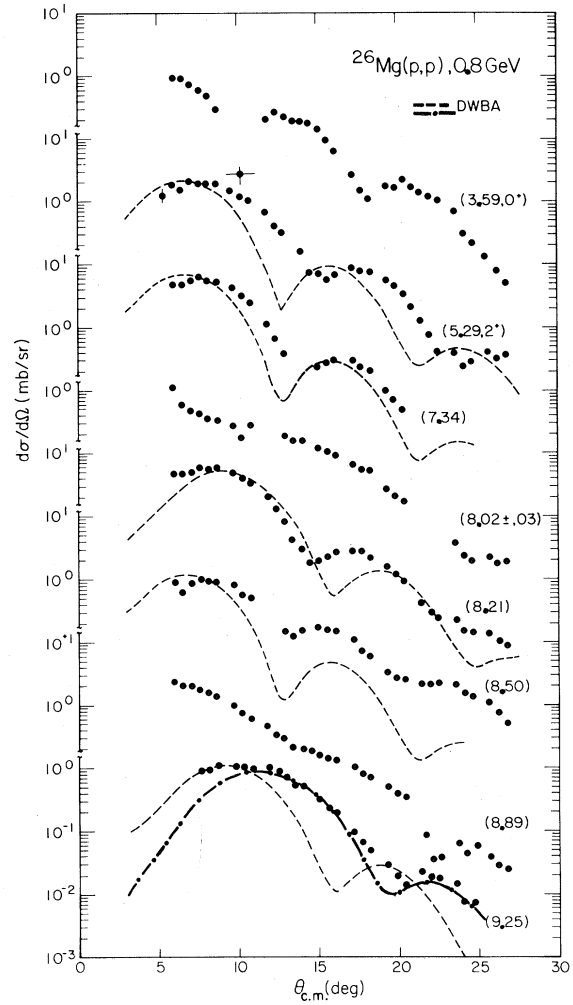


FIG. 14. Experimental angular distributions and DWBA predictions for various peaks in the $^{26}\text{Mg}(p,p')$ spectra. The deformation parameters and assumed l values are given in the text. An $l=4$ DWBA prediction (dot-dashed curve) is compared to the 9.25 MeV data where $|\beta_4 R| = 0.36$ fm.

several states of different J^π and comparable strength are experimentally summed together.

V. SUMMARY AND CONCLUSIONS

Measurements of the angular distributions for 0.8 GeV proton elastic and inelastic scattering to many excited states in ^{24}Mg and ^{26}Mg have been presented. Coupled-channels calculations assuming the collective rotational model provide excellent descriptions of the data for the lowest 0^+ , 2^+ , and 4^+ states, demonstrating the applicability of this

model to ^{24}Mg and ^{26}Mg . The importance of $\alpha_{42}(Y_{42} + Y_{4-2})$ vibrational coupling between the ground state and the 4_{γ}^{+} state which was found to be crucially important in ^{24}Mg (p, p') is also seen to be significant for ^{26}Mg (p, p'). Good fits to the (2.94, 2^{+}), (3.94, 3^{+}), and (4.9, 4^{+}) states in ^{26}Mg are obtained when this extra coupling is included. Several 3^{-} states are observed in both nuclei, the angular distributions of which demonstrate a striking K dependence which is well described by the coupled-channels calculations assuming the collective deformed-vibrational model with K^{π} equal to either 0^{-} or 3^{-} . Difficulties were encountered in fitting the (8.12, 6^{+}) state and the 0_{β}^{+} , 2_{β}^{+} , and 4_{β}^{+} states in ^{24}Mg .

The calculated inelastic transition to the 4_{γ}^{+} state in the $K^{\pi}=2^{+}$, γ band describes the 4.9 MeV data in ^{26}Mg quite well, but gives an inferior reproduction of the data for the (5.47, 4^{+}) and (5.72, 4^{+}) states. The importance of K mixing in the complicated excited state spectrum of ^{26}Mg has been investigated in Ref. 33 but was not considered in the calculations presented here.

Multipole moments of the empirical, deformed optical potentials are related to those of the deformed matter densities by Satchler's theorem and are compared to results obtained with other hadronic probes and to the multipole moments of the

charge densities obtained via electromagnetic measurements. In general, the deduced $M(E2, \text{matter})$ moments are 10–20% smaller than those of the charge densities. The results for ^{24}Mg and ^{26}Mg indicate that the deformations of the proton and neutron densities in ^{26}Mg are both reduced compared to ^{24}Mg .

Several new assignments of J^{π} for excited states in ^{26}Mg are made, based upon the distinctive l transfer dependence found in the position of the first maximum in the angular distributions. A total of seven 4^{+} states in ^{26}Mg are believed to have been observed.

It is hoped that these data will be used in future microscopic analyses that include deformed ground state densities. Measurements of π^{+} and π^{-} scattering from these isotopes at resonance energies are underway.^{35,36}

ACKNOWLEDGMENTS

The research reported here is supported in part by the U. S. National Science Foundation, the U. S. Department of Energy, and the Robert A. Welch Foundation. The authors would like to thank the LAMPF staff for their assistance in performing these measurements.

*Present address, SIN, 5234 Villigen, Switzerland.

†Present address, E. G. and G., Los Alamos, New Mexico 87544.

¹L. Ray, G. S. Blanpied, W. R. Coker, R. P. Liljestrand, and G. W. Hoffman, Phys. Rev. Lett. **40**, 1547 (1978).

²G. S. Blanpied *et al.*, Phys. Rev. C **23**, 2599 (1981).

³G. S. Blanpied *et al.*, Phys. Rev. C **20**, 1490 (1979).

⁴L. Ray, G. S. Blanpied, and W. R. Coker, Phys. Rev. C **20**, 1236 (1979).

⁵M. L. Barlett *et al.*, Phys. Rev. C **22**, 1168 (1980).

⁶G. R. Satchler, J. Math. Phys. **13**, 1118 (1972).

⁷Y. Horikawa, Y. Torizuka, A. Nakada, S. Mitsunobu, Y. Kojima, and M. Kimura, Phys. Lett. **36B**, 9 (1971).

⁸E. W. Lees *et al.*, J. Phys. A **7**, 936 (1974); and references contained therein.

⁹D. S. Schwalm *et al.*, Nucl. Phys. **A192**, 449 (1972); D. Schwalm, E. K. Warburton, and J. W. Olness, *ibid.* **A293**, 425 (1977).

¹⁰R. S. Mackintosh, Nucl. Phys. **A266**, 379 (1976).

¹¹R. M. Lombard, J. L. Escudie, and M. Soyeur, Phys. Rev. C **18**, 42 (1978).

¹²I. Lovas, M. Rogge, U. Schwinn, P. Turek, and D. Ingham, Nucl. Phys. **A286**, 12 (1977).

¹³J. Eenmaa, R. K. Cole, C. N. Waddell, H. S. Sandhu, and R. R. Dittman, Nucl. Phys. **A218**, 125 (1974).

¹⁴B. Zwiaglinski, G. M. Crawley, H. Nann, and J. A. Nolen, Jr., Phys. Rev. C **17**, 872 (1978).

¹⁵P. W. F. Alons, H. P. Blok, and J. F. A. van Hienen, Phys. Lett. **83B**, 34 (1979).

¹⁶R. De Leo *et al.*, Phys. Rev. C **23**, 1355 (1981).

¹⁷H. R. E. Tjin *et al.*, Nucl. Phys. **A106**, 85 (1968).

¹⁸N. M. Clarke, J. Phys. G **6**, 865 (1980).

¹⁹K. Van der Borg, M. N. Harakeh, and B. S. Nilsson, Nucl. Phys. **A325**, 31 (1979).

²⁰H. Rebel *et al.*, Nucl. Phys. **A182**, 145 (1972).

²¹Y. Abgrall, B. Morand, and E. Caurier, Nucl. Phys. **A192**, 372 (1972).

²²G. W. Hoffmann *et al.*, Phys. Rev. C **21**, 1488 (1980).

²³See AIP document No. PAPS PRVCS 25-422-45 for 45 pages of numerical data for 0.8 GeV scattering of

- protons from ^{24,26}Mg. Order by PAPS number and journal reference from American Institute of Physics, Physics Auxiliary Publications Service, 335 East 45th Street, New York, New York 10017. The prices are \$1.50 for microfiche or \$12.50 for photocopies. Air-mail additional. Make checks payable to the American Institute of Physics.
- ²⁴P. M. Endt and C. Van der Leun, Nucl. Phys. A310, 1 (1978).
- ²⁵L. Ray, W. R. Coker, G. W. Hoffmann, Phys. Rev. C 18, 2641 (1978); L. Ray, Phys. Rev. C 19, 1855 (1979).
- ²⁶D. M. Brink and G. R. Satchler, *Angular Momentum* (Oxford University Press, Oxford, 1968).
- ²⁷T. Tamura, Rev. Mod. Phys. 37, 679 (1965); T. Tamura, Oak Ridge National Laboratory Report No. ORNL-4152, 1967 (unpublished).
- ²⁸L. Ray, Phys. Lett. 102B, 88 (1981).
- ²⁹A. Johnston, and T. E. Drake, J. Phys. A 7, 898 (1974); O. Titze, Z. Phys. 220, 66 (1969).
- ³⁰J. L. Durell *et al.*, J. Phys. A 5, 302 (1972).
- ³¹A. Nagel *et al.*, J. Phys. A 14, 1697 (1974).
- ³²A. Nagel *et al.*, J. Phys. G 1, 324 (1975).
- ³³G. Craig, Nucl. Phys. A225, 493 (1974).
- ³⁴A. M. Bernstein, V. R. Brown, and V. A. Madsen, Phys. Rev. Lett. 42, 425 (1979).
- ³⁵Experiment 573 at LAMPF, using the EPICS system, G. Blanpied, spokesman.
- ³⁶C. A. Wiedner *et al.*, Phys. Lett. 97B, 37 (1980).